Appl Phys A (2009) 97: 735–740
DOI 10.1007/s00339-009-5438-1

Applied Physics A
Materials Science & Processing

RAPID COMMUNICATION

Inverse Method to estimate material parameters for piezoceramic disc actuators

Stefan J. Rupitsch · Reinhard Lerch

Received: 21 August 2009 / Accepted: 24 September 2009 / Published online: 8 October 2009

Abstract A novel Inverse Method for the determination of material parameters characterizing discoidal piezoceramic actuators is presented. In contrast to the common identification method, no specially shaped test samples are required. The Inverse Method is based on a finite element simulation. Both the measured mechanical and the electrical behavior of the actuator serve as input quantities of the new procedure. The presented results show the efficiency and correctness of the developed Inverse Method.

PACS 85.50.-n · 77.84.-s · 02.30.Zz · 07.05.Tp · 02.60.Cb

1 Introduction

There exists a variety of applications for piezoelectric devices such as ultrasound transducers for non-destructive evaluation (NDE) and medical imaging as well as transducers within smart materials [1–4]. So as to avoid time-consuming and expensive experiments, numerical simulation tools, namely finite element methods (FE), have been developed [5]. By means of FE simulations, both, the electrical as well as the mechanical behavior of the piezoelectric devices can be numerically determined [6, 7]. However, the correctness of these simulation results relies on appropriate material parameters, such as elastic moduli, dielectric constants and piezoelectric moduli.

The underlying research is gratefully founded by he German Research Foundation (DFG) as part of SFB/TR39.

S.J. Rupitsch (✉) · R. Lerch
Department of Sensor Technology,
Friedrich-Alexander-University Erlangen-Nuremberg,
Paul-Gordan-Strasse 3/5, 91052 Erlangen, Germany
e-mail: stefan.rupitsch@lse.eei.uni-erlangen.de

The commonly used piezoceramic materials for piezoelectric devices are of material class 6 mm (transversely isotropic). In the majority of cases, the material parameters for this class are determined according to the IEEE- or CENELEC-Standard [2, 8–10]. Therefore, various test samples with different geometries and directions of polarization are mandatory (Fig. 1). Since the test samples offer nearly monomodal vibrations, the whole parameter set can be determined. Nevertheless, due to principle shortcomings within the standard method (non monomodal vibrations of the test samples), the identified quantities may yield insufficient simulation results. Furthermore, the standard method is not applicable for numerous piezoelectric devices (e.g., piezoceramic-composites and piezo stack actuators), which do not allow the fabrication of the mandatory test samples.

In contrast to the common approach, we developed Inverse Methods, which do not require different test samples, but also allow the determination of the whole material parameter set. These methods are based on an adjustment of simulation to measurement results. So far, we used the frequency resolved electrical impedance of the piezoceramic device as input quantity of the Inverse Method [11, 12]. Unfortunately, several parameters only slightly influence the electrical impedance. On account of this fact, the identification of the complete material parameter set with the aid of Inverse Methods is hardly possible.

In this work, we additionally consider the spatially and frequency resolved surface normal velocities, which describe the local behavior of the actuator. As a matter of fact, the variation of every parameter causes a remarkable change of the surface normal velocities, even if the impedance remains unchanged. Thus, the consideration of both, the electrical impedances and velocities facilitates the determination of the whole material parameter set. In order to demonstrate

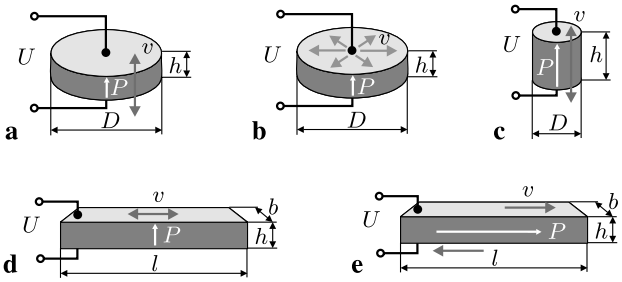

Fig. 1 (**a**) Thickness extensional mode; (**b**) radial mode; (**c**) longitudinal length mode; (**d**) transverse length mode; (**e**) thickness shear mode; excitation voltage U; polarization vector P

the efficiency of the developed Inverse Method, a discoidal piezoelectric actuator is investigated.

The paper is organized as follows. In Sect. 2, the numerical modeling of piezoelectric actuators is described. The Inverse Method, especially applied for discoidal actuators, is presented in Sect. 3. In Sect. 4, the achieved results are discussed.

2 Modeling of piezoelectric actuators

For small, electric fields and mechanical deformations, the piezoelectric effect can be modeled by [13]

$$\mathbf{T} = \left[\mathbf{c}^E\right]\mathbf{S} - [\mathbf{e}]^t\,\mathbf{E}, \tag{1}$$

$$\mathbf{D} = [\mathbf{e}]\,\mathbf{S} + \left[\boldsymbol{\varepsilon}^S\right]\mathbf{E}. \tag{2}$$

$\mathbf{T}$ and $\mathbf{S}$ denote the mechanical stress tensor (Voigt notation) and the mechanical strain tensor (Voigt notation), respectively. $\mathbf{E}$ stands for the electric field intensity and $\mathbf{D}$ relates to the dielectric displacement. The tensors for a 6 mm crystal of the elasticity coefficients $[\mathbf{c}^E]$, of the dielectric constants $[\boldsymbol{\varepsilon}^S]$, and of the piezoelectric coupling coefficients $[\mathbf{e}]$ are given by [1, 6]

$$\left[\mathbf{c}^E\right] = \begin{pmatrix} c_{11}^E & c_{12}^E & c_{13}^E & 0 & 0 & 0 \\ c_{12}^E & c_{11}^E & c_{13}^E & 0 & 0 & 0 \\ c_{13}^E & c_{13}^E & c_{33}^E & 0 & 0 & 0 \\ 0 & 0 & 0 & c_{44}^E & 0 & 0 \\ 0 & 0 & 0 & 0 & c_{44}^E & 0 \\ 0 & 0 & 0 & 0 & 0 & (c_{11}^E - c_{12}^E)/2 \end{pmatrix},$$

$$\left[\boldsymbol{\varepsilon}^S\right] = \begin{pmatrix} \varepsilon_{11}^S & 0 & 0 \\ 0 & \varepsilon_{11}^S & 0 \\ 0 & 0 & \varepsilon_{33}^S \end{pmatrix},$$

$$[\mathbf{e}] = \begin{pmatrix} 0 & 0 & 0 & 0 & e_{15} & 0 \\ 0 & 0 & 0 & e_{15} & 0 & 0 \\ e_{31} & e_{31} & e_{33} & 0 & 0 & 0 \end{pmatrix}.$$

These tensors show a certain symmetry and sparsity pattern [6]. Overall, the three tensors consist of 10 independent, non-vanishing entries, which are required in order to calculate the linearized electrical and mechanical behavior of the piezoceramic actuator. The dissipative losses are considered according to the Rayleigh damping model, which is common for the finite element method [11].

By means of Newton's law and Maxwell's equations, (1) and (2) can be transformed into coupled partial differential equations (PDE). This so-called strong formulation is adopted to the weak formulation with both, an appropriate test function as well as the necessary boundary conditions [6]. The finite element (FE) discretization scheme finally yields a linear system of equations.

3 Inverse Method

The Inverse Method is based on the best accordance of simulation and measurement results. During an iteration procedure the material parameters are adapted in a convenient way. The output quantity of the Inverse Method is a new set of material parameters.

The FE simulation of the electrical and mechanical behavior of the actuator yields the frequency resolved electrical impedance $\mathbf{Z}$ and frequency as well as spatially resolved surface normal velocity $\mathbf{v}$ (e.g., in thickness direction). Briefly, the simulation procedure can be abstractly formulated as so-called parameter-to-solution maps $\mathcal{F}_Z$ and $\mathcal{F}_v$ for the impedance and velocity, respectively:

$$\mathcal{F}_Z : \mathbb{R}^{n_{\text{par}}} \longrightarrow \mathbb{C}^{m_{\text{freq}}}, \qquad \mathcal{F}_Z(\mathbf{p}) = \mathbf{Z}, \tag{3}$$

$$\mathcal{F}_v : \mathbb{R}^{n_{\text{par}}} \longrightarrow \mathbb{C}^{n_{\text{freq}} \times o_{\text{x}}}, \qquad \mathcal{F}_v(\mathbf{p}) = \mathbf{v}. \tag{4}$$

$\mathbb{R}$ and $\mathbb{C}$ denote the set of real and complex numbers, respectively. The parameter vector $\mathbf{p}$ is composed of $n_{\text{par}} = 10$ components:

$$\mathbf{p} = \left(c_{11}^E, c_{12}^E, c_{13}^E, c_{33}^E, c_{44}^E, \varepsilon_{11}^S, \varepsilon_{33}^S, e_{31}, e_{33}, e_{15}\right). \tag{5}$$

Note that both, $\mathbf{Z} = [\underline{Z}(f_1), \ldots, \underline{Z}(f_{m_{\text{freq}}})]^t$ as well as $\mathbf{v} = [\underline{v}(\mathbf{x}_1, f_1), \ldots, \underline{v}(\mathbf{x}_{o_{\text{x}}}, f_{n_{\text{freq}}})]^t$ consist of complex-valued entries (real and imaginary part or magnitude and phase). The parameters m_{freq} and n_{freq} refer to the number of discrete frequencies. o_{x} stands for the number of points on the surface of the piezoelectric device.

3.1 Levenberg–Marquardt Method

With a view to determining the parameter set $\mathbf{p}$ of the piezoelectric actuator by means of matching simulation and measurement results, a modified Levenberg–Marquardt Method (LMM) is applied [14]. In contrast to the Gauss–Newton Algorithm, the LMM converges even for poor initial values. However, the speed of convergence for the LMM is rather slow. The LMM is based on the functional (iteration index (i))

$$\left\|\mathbf{F}'\left(\mathbf{p}^{(i)}\right)\mathbf{s}^{(i)}+\mathbf{F}\left(\mathbf{p}^{(i)}\right)\right\|_2^2+\mu^2\left\|\mathbf{s}^{(i)}\right\|_2^2\rightarrow\min., \tag{6}$$

which has to be minimized. The value of the parameter μ determines the speed of convergence. The larger μ, the slower the speed of convergence. The expression $\mathbf{F}(\mathbf{p}^{(i)})$ relates to the deviation of simulation $(\mathbf{Y}_\mathrm{S}(\mathbf{p}^{(i)}))$ and measurement results $(\mathbf{Y}_\mathrm{M})$ and is defined as

$$\mathbf{F}\left(\mathbf{p}^{(i)}\right)=\mathbf{Y}_\mathrm{S}\left(\mathbf{p}^{(i)}\right)-\mathbf{Y}_\mathrm{M}. \tag{7}$$

$\mathbf{F}'(\mathbf{p}^{(i)})$ denotes the Jacobian matrix (first order derivative of $\mathbf{F}(\mathbf{p}^{(i)})$ with respect to $\mathbf{p}$) at $\mathbf{p}^{(i)}$ and is determined with

$$\mathbf{F}'\left(\mathbf{p}^{(i)}\right)=\left.\frac{\partial\mathbf{F}(\mathbf{p})}{\partial\mathbf{p}}\right|_{\mathbf{p}=\mathbf{p}^{(i)}}=\left.\frac{\partial\mathbf{Y}_\mathrm{S}(\mathbf{p})}{\partial\mathbf{p}}\right|_{\mathbf{p}=\mathbf{p}^{(i)}}. \tag{8}$$

The minimum of (6) yields for the parameter correction vector $\mathbf{s}^{(i)}$

$$\mathbf{s}^{(i)}=\left[\mathbf{F}'\left(\mathbf{p}^{(i)}\right)^t\mathbf{F}'\left(\mathbf{p}^{(i)}\right)+\mu^2\mathbf{I}\right]^{-1}\times\mathbf{F}'\left(\mathbf{p}^{(i)}\right)^t\left(\mathbf{Y}_\mathrm{M}-\mathbf{Y}_\mathrm{S}\left(\mathbf{p}^{(i)}\right)\right), \tag{9}$$

where t is the transpose of the respective matrix. $\mathbf{I}$ in (9) stands for the identity matrix. Finally, the parameter vector $\mathbf{p}^{(i+1)}$ for the subsequent iteration step is given by

$$\mathbf{p}^{(i+1)}=\mathbf{p}^{(i)}+\mathbf{s}^{(i)}. \tag{10}$$

This procedure is continued until an appropriate stop criterion is fulfilled. The value of μ is decreased in subsequent iteration steps. Moreover, the considerable different magnitudes of the impedances and velocities require an appropriate scaling.

3.2 Sensitivity analysis

In order to obtain a feasible iteration procedure which is accompanied by reliable material parameters and a reasonable computation time a sensitivity analysis is performed. Thereby, the effect of parameter variations on the frequency resolved electrical impedance and on the spatially resolved surface normal velocity is investigated. The analysis was done for a piezoceramic discoidal actuator made of Pz27 with $D=25.2\,\mathrm{mm}$ in diameter and a height of $h=2.0\,\mathrm{mm}$ (Figs. 1(a) and (b)). Table 2 contains the material parameters for the actuator, which are provided by the manufacturer (*FERROPERM*).

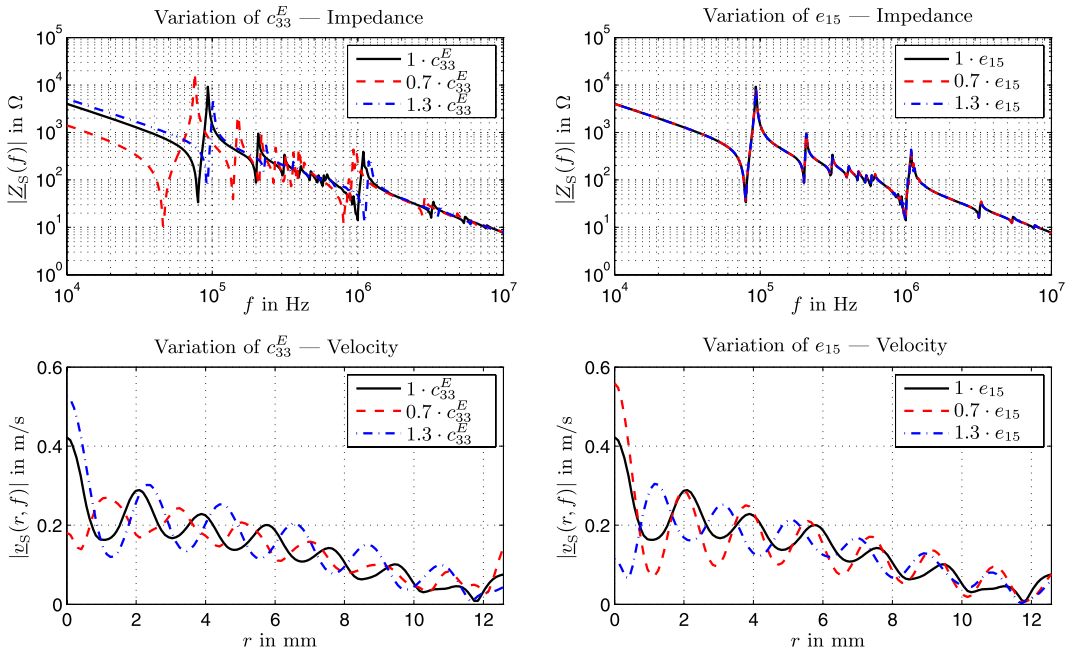

Fig. 2 Effect of the parameter variations for c_{33}^E (*left* panels) and e_{15} (*right* panels); (*top* panels) frequency resolved electrical impedances; (*bottom* panels) spatially resolved surface normal velocities for thickness resonance (thickness extensional mode; $U=10\,\mathrm{V_{pp}}$; $f=997.6\,\mathrm{kHz}$)

Table 1 Iteration sub-steps

Param. set **p**	Impedance radial	Impedance thickness	Velocity
Sub-Step 1 c_{33}^E, ε_{33}^S, e_{33}	■	■	■
Sub-Step 2 c_{11}^E, c_{12}^E, c_{13}^E	■	–	■
Sub-Step 3 c_{44}^E	–	■	■
Sub-Step 4 ε_{11}^S, e_{31}, e_{15}	–	–	■

Figure 2 shows the calculated frequency resolved electrical impedance and spatially resolved surface normal velocity (excitation voltage $U = 10\,\mathrm{V_{pp}}$) of the piezoelectric disc with respect to the parameter variation of c_{33}^E and e_{15}. The first and second resonance–antiresonance-pair in the electrical impedance relate to the resonance mode of the discoidal actuator in radial ($f \approx 100\,\mathrm{kHz}$) and thickness direction ($f \approx 1\,\mathrm{MHz}$), respectively (Figs. 1(a) and (b)). The spatially resolved surface normal velocity was calculated for the frequency $f = 997.6\,\mathrm{kHz}$, where the thickness resonance of the actuator for the manufacturer's parameter set occurs. In contrast to the variation of c_{33}^E, the variation of e_{15} has no effect on the impedance. However, the value of e_{15} influences the velocity. Hence, the consideration of both, the frequency resolved electrical impedance and spatially resolved surface normal velocity, is of utmost importance in order to obtain a reliable material parameter set for the actuator.

3.3 Iteration algorithm

So as to establish an iteration algorithm, the parameter analysis presented in the Sect. 3.2 was performed for the whole material parameter set of the discoidal actuator. The results clearly show, that a few parameters (c_{33}^E, ε_{33}^S, e_{33}) influence both, the frequency resolved electrical impedance as well as the spatially resolved surface normal velocity. However, there exist parameters (ε_{11}^S, e_{31}, e_{15}), which do not cause remarkable deviations of the impedance. Furthermore, the parameters influence different frequency bands of the impedance, namely the radial and thickness resonance.

The iteration procedure is arranged on the basis of the sensitivity analysis. As can be seen in Table 1, one iteration step consists of four sub-steps, whereas the parameter set **p** varies for each sub-step.

The vectors $\mathbf{Y}_\mathrm{M}$ and $\mathbf{Y}_\mathrm{S}$, which are required for the iteration procedure, consist of both, the frequency resolved electrical impedance as well as the frequency and spatially resolved surface normal velocity (11). The used frequency band ($f_{Z_1}, f_{Z_2}, \ldots, f_{Z_M}$) depends on the sub-step of the iteration algorithm.

$$\mathbf{Y}_\mathrm{M} = \begin{bmatrix} \mathbf{Z}_\mathrm{LM} \\ \mathbf{v}_\mathrm{M} \end{bmatrix}, \qquad \mathbf{Y}_\mathrm{S}(\mathbf{p}) = \begin{bmatrix} \mathbf{Z}_\mathrm{LS}(\mathbf{p}) \\ \mathbf{v}_\mathrm{S}(\mathbf{p}) \end{bmatrix}. \tag{11}$$

Due to the large value range, the absolute value of the electrical impedance $|\underline{Z}(f_{Z_i})|$ is logarithmized. The entries of the vectors for the measured ($\mathbf{Z}_\mathrm{LM}$) and calculated impedance ($\mathbf{Z}_\mathrm{LS}$) are defined as ($\log_{10} = \lg$)

$$\mathbf{Z}_{\mathrm{L\{M,S\}}} = \left[\lg\left(\left|\underline{Z}(f_{Z_1})\right|\right), \lg\left(\left|\underline{Z}(f_{Z_2})\right|\right), \ldots, \lg\left(\left|\underline{Z}(f_{Z_M})\right|\right)\right]^t.$$

According to the impedance, the vectors for the spatially resolved magnitudes of the measured ($\mathbf{v}_\mathrm{M}$) and calculated velocities ($\mathbf{v}_\mathrm{S}$) consist of the components

$$\mathbf{v}_{\mathrm{\{M,S\}}} = \left[\left|\underline{v}(\mathbf{x}_1, f_{v_1})\right|, \ldots, \left|\underline{v}(\mathbf{x}_O, f_{v_1})\right|, \left|\underline{v}(\mathbf{x}_1, f_{v_2})\right|, \ldots, \left|\underline{v}(\mathbf{x}_O, f_{v_2})\right|, \ldots, \left|\underline{v}(\mathbf{x}_1, f_{v_N})\right|, \ldots, \left|\underline{v}(\mathbf{x}_O, f_{v_N})\right|\right]^t.$$

The vector $\mathbf{x}$ denotes the spatial coordinate, namely the position in radial direction, on the surface of the discoidal actuator.

Note that for the fourth iteration sub-step, the electrical impedance is not considered. Hence, the electrical impedance is not part of the vectors $\mathbf{Y}_\mathrm{M}$ and $\mathbf{Y}_\mathrm{S}$.

4 Results

The presented Inverse Method was applied for a discoidal actuator (diameter $D = 25.2\,\mathrm{mm}$; height $h = 2.0\,\mathrm{mm}$) made of Pz27. The frequency resolved electrical impedance was measured with an impedance analyzer (*HEWLETT PACKARD* HP4194). The spatially resolved surface normal velocity was determined with a Laser-Scanning-Vibrometer (*POLYTEC* PSV300). As input quantities of the iteration algorithm, the electrical impedances in the frequency bands 50 kHz–150 kHz and 0.8 MHz–1.5 MHz were used. Moreover, the velocities in thickness direction for 850.0 kHz, 900.0 kHz, 950.0 kHz and 982.2 kHz were considered. The resonance frequency $f = 982.2\,\mathrm{kHz}$ for the thickness extensional mode was determined from the local minimum of the frequency resolved electrical impedance.

4.1 Results of the Inverse Method

Table 2 shows a comparison of the parameter set provided by the manufacturer and the result of the Inverse

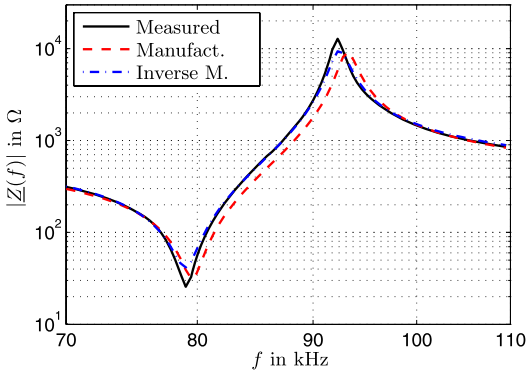

Fig. 3 Measured and calculated frequency resolved electrical impedances for the radial mode

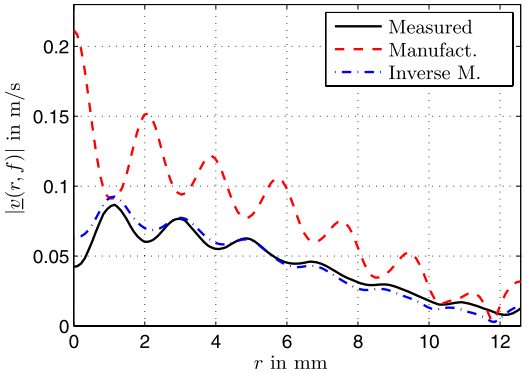

Fig. 4 Measured and calculated spatially resolved surface normal velocities for the thickness extensional mode ($U = 10\,\mathrm{V_{pp}}$; $f = 1.0\,\mathrm{MHz}$)

Table 2 Comparison of the material parameter set provided by the manufacturer and the results of the Inverse Method (c^E_{xy} in $\mathrm{N/m^2}$; ε^S_{xx} in $\mathrm{As/Vm}$; e_{xy} in $\mathrm{As/m^2}$); deviations related to manufacturer's material parameters

Param.	Manufacturer	Inverse Method	Deviations
c^E_{11}	1.47×10^{11}	1.34×10^{11}	−8.96%
c^E_{12}	1.05×10^{11}	7.97×10^{10}	−24.11%
c^E_{13}	9.37×10^{10}	8.19×10^{10}	−12.61%
c^E_{33}	1.13×10^{11}	1.12×10^{11}	−1.36%
c^E_{44}	2.30×10^{10}	1.99×10^{10}	−13.66%
ε^S_{11}	1.00×10^{-8}	9.31×10^{-9}	−6.88%
ε^S_{33}	8.09×10^{-9}	7.40×10^{-9}	−8.47%
e_{31}	−3.09	−3.48	12.71%
e_{33}	16.00	15.84	−0.99%
e_{15}	11.64	10.66	−8.41%

Method. As one can see, the deviations for the parameters are remarkable. For instance, the deviation for c^E_{12} is more than 20 %.

Figure 3 depicts the measured and calculated electrical impedances for the frequency band, where the radial resonance occurs. In contrast to the result of the Inverse Method, the material parameters from the manufacturer cause a slight frequency shift of the impedance.

4.2 Verification of the identified material parameters

In order to prove the results of the Inverse Method, the identified material parameters were used to calculate the spatially resolved surface normal velocity for $f = 1.0\,\mathrm{MHz}$. Note that the velocities at this frequency were not considered in the iteration procedure. Figure 4 shows a comparison of the measurement and simulation results. In contrast to the velocities obtained with the identified material parameters, the manufacturer's material parameters yield significant deviations. Hence, these material parameters are only limited suitable to simulate the electrical and mechanical behavior (Fig. 4) of the investigated discoidal actuator.

5 Conclusion

The proposed simulation based Inverse Method provides suitable material parameters for the investigated discoidal piezoceramic actuator. In contrast to our previous work, both, the frequency resolved electrical impedance as well as the frequency and spatially resolved surface normal velocity serve as input quantity of the Inverse Method. Thus, the determination of the complete parameter set for the piezoceramic material is facilitated. The Inverse Method consists of four sub-steps with different parameter sets, which are composed on the basis of a sensitivity analysis. As the presented results showed, both, the mechanical as well as the electrical behavior, can be calculated by means of the identified material parameters. Further work will be concentrated on modified Inverse Methods, which can be applied for other actuator shapes, e.g., block shaped piezoceramic actuators.

References

1. R. Lerch, G.M. Sessler, D. Wolf, *Technische Akustik* (Springer, Berlin, 2009)
2. W. Heywang, K. Lubitz, W. Wersing, *Piezoelectricity: Evolution and Future of a Technology* (Springer, Berlin, 2009)
3. S.J. Rupitsch, B.G. Zagar, IEEE Trans. Instrum. Meas. **56**(4), 1429 (2007)
4. K.H. Lam, H.L.W. Chan, J. Appl. Phys. A **81**(7), 1451 (2005)
5. R. Lerch, IEEE Trans. Ultrason. Ferroelectr. Freq. Control **37**(2), 233 (1990)
6. M. Kaltenbacher, *Numerical Simulation of Mechatronic Sensors and Actuators* (Springer, Berlin, 2007)
7. R. Paradies, B. Schläpfer, Smart Mater. Struct. **18**(2), 025015 (2009)
8. M. Wiesner, Eur. Phys. J. Appl. Phys. **28**(2), 243 (2004)

9. X.H. Du, Q.M. Wang, K. Uchino, IEEE Trans. Ultrason. Ferroelectr. Freq. Control **51**(2), 227 (2004)
10. X.H. Du, Q.M. Wang, K. Uchino, IEEE Trans. Ultrason. Ferroelectr. Freq. Control **51**(2), 238 (2004)
11. T. Lahmer, M. Kaltenbacher, B. Kaltenbacher, R. Lerch, E. Leder, IEEE Trans. Ultrason. Ferroelectr. Freq. Control **55**(2), 465 (2008)
12. T. Lahmer, J. Inv, Ill-Posed Problems **17**, 51 (2009)
13. W.P. Mason, *Physical Acoustics—Principles and Methods* (Academic Press, New York, 1964)
14. G.A. Watson, J.J. Móre, *Numerical Analysis: The Levenberg-Marquardt Algorithm* (Springer, Berlin, 1978), pp. 105–116